DESIGN AND CONSTRUCTION OF SUPPORT FACILITIES FOR MIRCO-CONCRETE MODEL SHELLS, HYPERBOLOIDS OF REVOLUTION

by

THOMAS EDWARD GATES

B.S., Kansas State University, 1979

A MASTER'S THESIS

submitted in partial fulfillment of the

requirements for the degree

MASTER OF SCIENCE

Department of Civil Engineering

KANSAS STATE UNIVERSITY
Manhattan, Kansas

1981

Approved by:

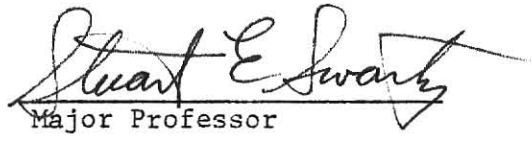

Major Professor

THIS BOOK
CONTAINS
NUMEROUS PAGES
WITH THE ORIGINAL
PRINTING BEING
SKEWED
DIFFERENTLY FROM
THE TOP OF THE
PAGE TO THE
BOTTOM.

THIS IS AS RECEIVED
FROM THE
CUSTOMER.

Table of Contents

List of Tables

Page

List of Figures

(P)--Photo

Synopsis

The size of hyperboloids of revolution of reinforced concrete used for natural-draft cooling towers has increased from 115 ft. (35m) in 1914 to 495 ft. (151 m) in 1979 with a height of 656 ft. (200 m) or more under consideration for the near future. With the advent of high strength concrete, precasting techniques for certain elements, and innovative construction techniques, elemental wall thicknesses as small as 2.5 in (0.06 m) are anticipated with 5.5 to 6.5 in (0.14-0.16 m) currently being used.

Due to these trends and following the collapse of three 370 ft. (113 m) towers on November 1, 1965 during high winds, a considerable interest in determining the buckling behavior of such thin walled shells under the loadings normally encountered has developed.

An extensive body of knowledge exists concerning the buckling analysis of such shells under loadings (4,9)* as well as studies on small elastic models (4,9,17). However, no information has appeared on physical testing of concrete models.

The work described, herein, is on the design and construction of support facilities for the testing of micro-concrete hyperboloids of revolution. These shells were proportioned to exhibit buckling prior to general collapse under loadings which include uniform and non-uniform lateral pressure and axial load.

The shells are 0.5 in (13 mm) thick, 12 ft. (3.65 m) high, and 9.33 ft. (2.84 m) in diameter at the base. These are proportioned within the range of those used in practice and the elastic models reported in References 9 and 17.

A fairly simple system for monitoring surface displacements under the action of either surface loads or axial compression and for measuring initial surface imperfections is also described.

---

* Parenthesis refer to items listed in Bibliography.

Chapter I

Introduction

Natural-draft hyperboloids of revolution cooling towers of reinforced concrete have increased in size from 115 ft. (35 m) in 1914 to 495 ft. (151 m) in 1979 with a height of 656 ft (200 m) or more under consideration for the near future. Currently elemental wall thicknesses of 5.5 in (0.14 m) to 6.5 in. (0.16 m) are being used, however, with the advent of high-strength concrete, precasting techniques for certain elements, and innovative construction techniques wall thickness as small as 2.5 in. (0.06 m) are anticipated.

Due to these trends and following the collapse of three 370 ft (113 m) cooling towers at Ferrybridge, England in 1965 during high winds (6), numerous analytical studies on determining the buckling behavior of such thin walled shells under loadings have been presented (7,8,9,15,21,22,23) as well as studies on experimental elastic models (4,11,17). Tentative design recommendations have resulted from these studies (1,13).

A summary of results of these studies is presented by Cole, et. al. (9) in terms of pertinent shell parameters. These geometry parameters are displayed in Table 1 along with those from more recent studies (17,23). Further, motivation for the numerous studies, including the present, are given by

1. Better understanding of buckling behavior and the primary factors affecting it. In addition to the buckling loads, careful experiments yield the behavior of the shell just prior to, at, and after buckling and accentuate the main parameters affecting this behavior.
2. To obtain better inputs for computations. Mathematical models employed in large multi-purpose computer programs can closely simulate real shell structures, but the simulation depends on the appropriate structural model, input

of the correct boundary conditions, imperfections, and load applications. These inputs can be provided by appropriate nondestructive tests.

3. To obtain correlation factors between analysis and test and for the material effects. Test results still differ considerably from predictions even when large programs are employed. These differences are partly due to the inaccuracies of inputs, to incomplete simulation, or to variations in buckling behavior or the mathematical model and the shells tested. These variables can be lumped into a correlation factor. The advantage of such a factor is the overall correlation it provides for the designer, but its weakness is that it is completely reliable only for the shells tested.

In all of the model studies listed, the shells were made of an elastic, homogeneous material. No information has appeared in the literature, to date, describing tests on concrete shell models. This fact and the novel idea of the formwork construction for the model shells distinguish the current study from others. It is felt that the influences of cracking, composite action and non-linear material properties on shell stress distributions and buckling behavior may be significant.

The design and construction of support facilities for micro-concrete model shells, hyperboloids of revolution are presented. A total of eight models with varying support conditions, thickness, loading conditions and reinforcement configurations are to be constructed and tested in the future.

Based on previous studies as described in Chapter II Review of Literature the shell model was proportioned such that failure would be initiated by buckling. The final dimensions selected using buckling equations developed by membrane theory in Chapter III Theoretical Background-Shell Model were a

overall shell height, H=12 ft (3.65 m); shell throat radius, a=3 ft. (0.91 m); shell thickness, h=0.25 to 0.5 in (6.5-13 mm); and shell geometry parameter, b=7.55 ft (2.30 m).

Details of construction of the formwork, special loading arrangements, and special instrumentations are given in Chapter IV Design of Equipment.

Chapter II

Review of Literature

There is little available information in the literature on the behavior of concrete shells, hyperboloids of revolutions. Hyperboloids of elastic, isotropic material subjected to wind loads and gravity loads are analyzed with respect to buckling in References 15 and 20. A recent summary of work in the area of buckling of hyperboloids is given in Reference 9.

Experimental studies have been primarily on small elastic models (4,11,17) or by numerical methods (7,8,21,22). To cite a few of these, Der and Fidler (11) have carried out an extensive series of tests in a compressed air wind tunnel and have investigated such factors as cornice rings, vertical and horizontal cracking, and the grouping of several towers. Chan and Firman (7,8) used a geometrically nonlinear finite element analysis with an incremental load procedure during their study of hyperboloidal model towers. The asymptote of the nonlinear load-deflection curve is the critical value of the nonaxisymmetric wind pressure. Finally, Yeh (22) has used quadrilateral finite elements to study the geometrically nonlinear dynamic response of a prototype hyperboloid tower. Using a fixed form of wind time-history and varying the amplitude of the pressure, he was able to determine the pressure magnitude which causes the displacement to become unbounded at some time during the response. These studies generally have shown that the predicted buckling loads are in poor agreement with those measured experimentally. Further, the models were not proportioned such that failure was initiated by buckling.

The usual proportions used in design are such that buckling need not be considered, and this perhaps is one reason so few concrete thin shells have been tested. Also there are very few theoretical analyses available for predicting buckling in concrete shells. However, with the use of high-

strength concrete and better fabrication procedures the trend is toward larger thinner shells with a correspondingly greater propensity towards failure by buckling.

Chapter III

Theoretical Background-Shell Model

1. Shell Geometry

A hyperboloid of revolution is a surface with three planes of symmetry, such that plane sections parallel to either of two planes of symmetry are hyperbolas. When a hyperbola is rotated about its real axis a hyperboloid of one sheet results. Being a surface of revolution a circular cross sections is characteristic.

Standard notion for pertinant shell geometric parameters is shown in Fig. 1 for a typical shell (18,20). If its symmetry axes are taken as X,Y, and Z axes, the hyperboloid of one sheet can be given the equation (18)

$$\frac{X^2}{a^2} + \frac{Y^2}{a^2} - \frac{Z^2}{b^2} = 1 \ . \tag{1}$$

Substituting $r^2 = X^2 + Y^2$ into (1) we obtain

$$\frac{r^2}{a^2} - \frac{Z^2}{b^2} = 1 \ , \tag{2}$$

or,

$$r = a\sqrt{1 + \frac{Z^2}{b^2}} \ , \tag{3}$$

in which r is the horizontal radius, z is the vertical coordinate, a is the throat radius and

$$b = \frac{aH_T}{\sqrt{R_B^2 - a^2}} \ . \tag{4}$$

In the above, R_B is the base radius, and H_T is the vertical distance from the throat to the base.

Using coordinate Ø the principal radii are (18, 20)

$$R_{\phi} = -a^2b^2\left(\frac{r^2}{a^4} + \frac{Y^2}{b^4}\right)^{3/2} ,$$

$$= -\frac{a^2b^2}{(a^2 \sin^2 \phi - b^2 \cos^2 \phi)^{3/2}} , \tag{5}$$

$$R_{\theta} = a\left\{1 + \frac{Y^2}{a^2}\left[\frac{b^2}{a^2} + \left(\frac{b^2}{a^2}\right)^2\right]\right\}^{1/2} ,$$

$$= \frac{a^2}{(a^2 \sin^2 \phi - b^2 \cos^2 \phi)^{1/2}} , \tag{6}$$

and,

$$r = \frac{a^2 \sin \phi}{(a^2 \sin^2 \phi - b^2 \cos^2 \phi)^{1/2}} ,$$

$$= R_{\theta} \sin \phi . \tag{7}$$

In the above

$$\text{Tan } \phi = \pm \frac{b}{a}\sqrt{\frac{r^2}{r^2 - a^2}} ,$$

$$= \pm \frac{b}{a}\sqrt{1 + \frac{b^2}{Z^2}} . \tag{8}$$

The most striking property of the hyperboloid of one sheet is that it contains two sets of straight (ruling) lines. No two lines of either set are coplanar, and each line of each set intersects each line of the other. Through each point of the surface passes one line of each set, and the two lines passing through each point determine the tangent plane at that point. Considering the intersection with the shell of a plane tangent to the shell surface at the throat (Z=0 and X=a) the equation of these ruling lines, from equation (1) is

$$\frac{Y^2}{a^2} - \frac{Z^2}{b^2} = 0 ,$$

or,

$$Y = \pm \frac{a}{b} Z \quad . \tag{9}$$

The slope of each line as viewed in the Y-Z or r-Z plane is

$$\text{Tan } \phi_r = \frac{dY}{dz} = \pm \frac{a}{b} \, . \tag{10}$$

To obtain a pattern of circumferential holes at different levels through which a ruling line will pass consider the plan view of a shell shown in Fig. 2. To construct a ruling line on the shell surface going from the base ($r=R_B$) to some level above the throat, e.g. lines A-1 or B-2, the line is visualized as passing originally through points A-1' or B-2'. The final hole alignment is yielded by rotating the upper circle through an angle δ.

The length of the ruling line may be obtained from

$$L^2 = (H_T - Z)^2 + (\sqrt{R_B^2 - a^2} + \sqrt{r^2 - a^2})^2 \, , \tag{11}$$

and the angle δ from

$$\cos \delta = \frac{a^2 - \sqrt{(R_B^2 - a)^2 (r^2 - a^2)}}{rR_B} \, , \tag{12}$$

for $Z \leq 0$.

The angle α and γ may be easily determined from Fig. 2 to be

$$\cos \alpha = \frac{a}{R_B} \, , \tag{13}$$

and,

$$\gamma = 2(\delta - \alpha) \quad . \tag{14}$$

2. Membrane Theory

For the shells considered here, two simplifications are often admissible: (1) the membrane stress theory and (2) a simplified bending theory. The principle guide for the choice of a theory is the successful long-term structural behavior of the type of thin shell and its scale. Very simplified theories have proved successful for dome roofs under gravity loading and circular cylindrical walls under internal pressure (20).

Analysis is commonly based on the following assumptions:

1. The material is homogenous, isotropic, and linearly elastic. Although none of these assumptions is correct for concrete, tests have indicated that under working loads, the concrete thin shell behaves very nearly as if they were.
2. The system behaves according to the small-deflection theory; requires that deflections under load be small enough so that changes in geometry do not alter the static equilibrium. The measure of validity for this theory is that the radial displacements of the shell be small compared with its thickness.
3. The thickness of a thin shell is denoted by h and is always considered small in comparison with its radius of curvature r.
4. The in-plane forces are distributed uniformly over the thickness. They are often expressed as stress resultants, defined as forces per unit length on the middle surface. A stress resultant divided by h yields a stress. Membrane stress resultants are denoted by N_X, N_Y, and $N_{XY} = N_{YX}$ and can be obtained solely from equations of equilibrium. See Fig. 1.

The membrane theory is based upon the assumption of no bending or transverse shear in the shell; only in-plane forces are considered. In many thin shells this provides a reasonable basis for design except at the boundaries where the shell is supported or stiffened. This is due to local restraints existing at the boundaries, or because the edge member cannot supply the reactions required by the membrane theory. The substantial bending that can occur at the boundaries is usually evaluated by an approximate bending theory in which the effects of edge loads and edge displacements on both stress resultants and bending moments are considered.

The differential equations of equilibrium of a shell of revolution based on membrane theory are well known (18) and given by

$\Sigma F_\theta = 0$:

$$\frac{1}{R_\phi}\frac{\partial N_{\phi\theta}}{\partial \phi} + 2\frac{\cot\phi}{R_\theta}N_{\phi\theta} + \frac{1}{R_\theta \sin\phi}\frac{\partial N_\theta}{\partial \theta} + P_\theta = 0 \quad ,$$

or,

$$\frac{\partial N_\theta}{\partial \theta}R_\phi + N_{\theta\phi}R_\phi \cos\phi + \frac{\partial}{\partial \phi}(N_{\phi\theta}R_\theta \sin\phi) + P_\theta R_\phi R_\theta \sin\phi \; . \qquad (15)$$

$\Sigma F_\phi = 0$:

$$\frac{1}{R_\phi}\frac{\partial N_\phi}{\partial \phi} + \frac{\cot\phi}{R_\theta}(N_\phi - N_\theta) + \frac{1}{R_\theta \sin\phi}\frac{\partial N_{\phi\theta}}{\partial \theta} + P_\phi = 0 \quad ,$$

or,

$$\frac{\partial}{\partial \phi}(N_\phi R_\theta \sin\phi) - N_\theta R_\phi \cos\phi + \frac{\partial N_{\theta\phi}}{\partial \theta}R_\phi + P_\phi R_\phi R_\theta \sin\phi = 0 \; . \qquad (16)$$

$\Sigma F_n = 0$:

$$\frac{N_\phi}{R_\phi} + \frac{N_\theta}{R_\theta} - P_n = 0 \; ,$$

or,

$$N_\phi R_\theta + N_\theta R_\phi - P_n R_\phi R_\theta = 0 \quad , \qquad (17)$$

where P_ϕ, P_θ, and P_n are the load components per unit area of middle surface.

Self Weight

The components of the dead load are given by

$$P_\theta = 0, \; P_\phi = g \sin\phi, \; P_n = -g\cos\phi \; , \qquad (18)$$

for shells of constant thickness, in which g is the dead weight per unit area of the surface. Due to symmetry of the loads, $N_{\phi\theta} = N_{\theta\phi} = 0$, and all terms involving derivatives with respect to θ vanish. Inserting these and the components of (18) into Equations (16) and (17) the following equations of equilibrium will be obtained

$\Sigma F_n = 0$:

$$\frac{N_\phi}{R_\phi} + \frac{N_\theta}{R_\theta} = -g \cos \phi \quad ,$$

$$N_\theta = \frac{-R_\theta}{R_\phi} N_\phi - g R_\theta \cos \phi \quad . \tag{19}$$

$\Sigma F_\phi = 0$:

$$\frac{d}{d\phi} (N_\phi R_\theta \sin\phi) - N_\theta R_\phi \cos\phi + P_\phi R_\phi \sin\phi = 0 \quad ,$$

$$N_\phi = \frac{-g}{4} b^2 \sqrt{a^2 + b^2} \frac{\sqrt{(1 - \xi^2)}}{(a^2+b^2-a^2\xi^2)} [f(\xi) - f(\xi_T)] \quad , \tag{20}$$

where the parameter ξ is determined from

$$\xi = \sqrt{1 + \left(\frac{b}{a}\right)^2} \cos\phi \quad , \tag{21}$$

and,

$$f(\xi) = \frac{2\xi}{1-\xi^2} + \ln \frac{1 + \xi}{1 - \xi} \tag{22}$$

Uniform External Pressure

Similar to the dead load for shells of constant thickness, the components of uniform external pressure are given by

$$P_\theta = P_\phi = 0, \quad P_n = -q \quad . \tag{23}$$

Due to symmetry of the loads, $N_{\phi\theta} = N_{\theta\phi} = 0$, and all terms involving derivatives with respect to θ vanish. Inserting these and the components of (23) into Equations (16) and (17) the following equations of equilibrium will be obtained

$\Sigma F_n = 0$:

$$\frac{N_\phi}{R_\phi} + \frac{N_\theta}{R_\theta} = -q \quad ,$$

$$N_\phi = \frac{-R_\theta}{R_\phi} N_\phi - R_\theta q \quad . \tag{24}$$

$\Sigma F_\phi = 0$:

$$\frac{d}{d\phi} (N_\phi R_\theta \sin\phi) - N_\theta R_\phi \cos \phi = 0 \quad ,$$

$$N_\phi = \frac{-qa^2}{2b} \frac{\sqrt{\zeta}}{(1+\zeta)} (\zeta - \zeta_T) \quad , \tag{25}$$

where,

$$\zeta = \frac{b^2}{a^2 \sin^2\phi - b^2\cos^2\phi} \quad . \tag{26}$$

Vertical Load at Top of Shell

The components due to a total downward axial load applied uniformly along the circumference, $2\pi R_{TOP}P$, at the top of the shell are given by

$$P_\phi = P_\theta = P_n = 0 \quad . \tag{27}$$

Due to the downward axial load $N_{\phi\theta} = 0$, and $N_\phi(\phi)$ is independent with respect to θ. Using these relationships and summing forces with respect to n and Z, the following equations of equilibrium will be obtained

$\Sigma F_n = 0$:

$$R_\phi N_\theta + R_\theta N_\phi = 0$$

$$N_\theta = \frac{-R_\theta}{R_\phi} N_\phi \tag{28}$$

$\Sigma F_Z = 0$:

$$P(2\pi R_{TOP}) + (N_\phi \sin\phi)(2\pi r) = 0 \quad ,$$

$$N_\phi = \frac{-PR_{TOP}}{r\sin\phi} \quad . \tag{29}$$

Wind Load

Membrane stress resultants for wind loading are not easily computed since the load is not axisymmetrical. Critical for design, the meridional stress resultant must be considered.

Expressions for other membrane forces, notably due to wind loads may be found in References 18 and 20.

3. Shell Stresses and Buckling Loads

Numerous methods are available for estimating the load at which local buckling in the shell will commence (4,7,8,9,13,15,17). Although non-

linear load-displacement response is considered these all assume linear material response as stated previously.

Recommended by the I.A.S.S. Working Group (13), the stability criterion against local buckling using only the membrane stresses will be used. The membrane solution determined from Equations (18) - (29) are assumed to be calculated with sufficient accuracy, as an initial trial, for the case of symmetrically-applied loads. Future work will include evaluation of these stresses using a suitable bending theory.

The stability criterium against local buckling may be represented by

$$0.8\left[\frac{\tilde{\sigma}\theta}{\sigma\theta_o}+\frac{\tilde{\sigma}\phi}{\sigma\phi_o}\right]+0.2\left[\left(\frac{\tilde{\sigma}\theta}{\sigma\theta_o}\right)^2+\left(\frac{\tilde{\sigma}\phi}{\partial\phi_o}\right)^2\right]=1 \quad , \tag{30}$$

in which,

$$\tilde{\sigma}\theta=\frac{-N_\theta}{h}\ ,\ \tilde{\sigma}\phi=\frac{-N_\phi}{h}\ ,$$

and,

$$\sigma\theta_o=Q_\theta E_T\ ,\ \sigma\phi_o=Q_\phi E_T\ .$$

To account for the non-linear stress-strain response of concrete the stability criterium has been modified using the Tangent Modulus buckling concept where Young's Modulus, E, is replaced by a tangent modulus, E_T.

The geometry buckling parameters Q_θ and Q_ϕ are given by (17)

$$\begin{Bmatrix}Q_\theta\\Q_\phi\end{Bmatrix}=\frac{1}{(1-\nu^2)^{3/4}}\left(\frac{h}{a}\right)^{4/3}\begin{Bmatrix}K_{G\theta}\ F_\theta\\K_{G\phi}\ F_\phi\end{Bmatrix} \quad , \tag{31}$$

in which ν is Poisson's Ratio; $K_{G\theta}$, $K_{G\phi}$ are factors depending on the shape and boundary conditions of the cooling tower shell obtained using bifurcation theory; and F_θ, F_ϕ are experimental correction factors depending on the shape of the cooling tower shell. These factors are given for a wide range of shell geometry parameters by Almannai and Mungan (4,13).

In the development of the buckling formulas an applied axial load is assumed to be present due to the top plate incorporated for loading the

shell during testing. This load is related to the lateral pressure (internal suction) by $P = 1/2\ \lambda q R_{TOP}$, $0 \leq \lambda \leq 1.0$.

The formula for the pressure at which buckling commences is given by

$$q_{cr} = \frac{2\bar{q}_{cr} f'_c}{\varepsilon_o}\left[\frac{-N\bar{q}_{cr}}{\varepsilon_o} + \sqrt{1 + \left(\frac{N\bar{q}_{cr}}{\varepsilon_o}\right)^2}\right], \tag{32a}$$

when N_θ dominates, and

$$q_{cr} = \frac{2\bar{q}_{cr} f'_c}{\varepsilon_o}\left[\frac{-M\bar{q}_{cr}}{\varepsilon_o} + \sqrt{1 + \left(\frac{M\bar{q}_{cr}}{\varepsilon_o}\right)^2}\right], \tag{32b}$$

when N_ϕ dominates.

In the above, f'_c and ε_o are the concrete uniaxial compressive strength and associated strain, respectively.

The term $\bar{q}_{cr}$ is given by

$$\bar{q}_{cr} = \frac{1}{S^2 + T^2}\left[-2(S+T) + \sqrt{9S^2 + 8ST + 9T^2}\right], \tag{33}$$

where,

$$S = \frac{N}{Q_\theta}, \quad T = \frac{M}{Q_\phi},$$

and,

$$M = \frac{1}{h\sin^2\phi}\left[\frac{a^2(\zeta - \zeta_T)}{2bK^2\sqrt{\zeta}} + \frac{\lambda R_{TOP}^2}{2R_\theta}\right], \tag{34}$$

$$N = R_\theta\left(\frac{-M}{R_\phi} + \frac{1}{h}\right). \tag{35}$$

The term ζ is given by Eq. (26) and $k^2 = 1 + \frac{a^2}{b^2}$.

The formula for q_{cr} is to be applied for various values of Z to obtain a minimum value. Alternatively, based on experience or observation the calculation is made at the location that the surface has buckled previously.

Buckling Load

A micro-concrete specimen with ultimate compressive strength f'_c = 4,000 psi (27.6 MPa) and associated strain ε_o = 0.002 in/in (m/m) was assumed for estimating buckling loads and associated stresses for the proposed shell model. A

typical unit weight for concrete of 150 lb/ft^3 (23.8 k N/m^3) was also assumed.

Presented in Table 2 are results for the proposed shells of three thickness - 0.5 in (13 mm), 0.375 in (10 mm) and 0.25 in (6 mm). These were determined directly from Eqs. (30) to (35). The force N_θ dominates in all cases, implying a type of ring buckling. Further, the self-weight forces are quite low compared to those due to lateral pressure and axial load at buckling. Hence, these were neglected in the development of the buckling formulas previously.

The results of the calculations are presented in each case for locations in the shell at the throat, one-third the way from the throat to the base, and at the base. It is seen that the loads vary approximately as the square of the wall thickness.

It is also seen that the lowest loads are associated with the membrane stress state at the base. Described previously, the membrane solution is not sufficiently accurate at this location due to the base restraint, assumed to be fixed or stiffened by a ring beem.

Based on observations reported on tests of elastic models as well as analytical results indicate the buckled region to be somewhat below the throat.

Taking the load results for the region Z=36 in (91 cm) the stresses in each shell due to dead load g, pressure q, and axial load P were calculated and are presented in Table 3.

These results indicate the following:

1. Due to self-weight, g, the stresses are independent of shell thickness and also are very small in comparison to the stresses due to the other loads.
2. The total stresses associated with the buckling loads vary almost in direct proportion to the shell thickness.

Chapter IV

Design of Equipment

1. Shell Model

The model which is shown in Fig. 1 was proportioned such that failure will be initiated by buckling and with the following considerations.

1. It is estimated that the wall thickness must be 0.25 in (6.5 mm) to 0.50 in (13 mm) as not to preclude steel placement with sufficient cover and adequate steel ratio.
2. Based on previous studies the remaining dimensions should give proportions within the range of values shown in Table 1.

The dimensions selected yield the following

$$\frac{H}{a} = 4.0 \ , \ \frac{a}{h} = 72 \text{ to } 144 \ , \ \frac{a}{b} = 0.397$$

or H=12 ft (3.65 m), overall shell height; a=3 ft (0.91 m) shell throat radius; h=0.25 to 0.5 in (6.5-13 mm), shell thickness; and b=7.55 ft. (2.30 m), shell geometry parameter. It can be seen that these values correspond well with References (7,8,11,15) and (22) as listed in Table 1, hence correlation of results would be expected.

The top plate shown in Fig. 16 rests on a steel column (HP 10x45) and seals the top of the shell so that a uniform load may be applied by suction. Based on plate bending theory (20) the column will take approximately 44% of the total load and the total axial load taken by the shell wall is $0.56\pi R_{TOP}^2 q$. Thus, the load per unit length of shell wall is

$$P = 0.28 \, R_{TOP} q \tag{36}$$

or, $\lambda = 0.56$.

2. Model Material

Micro-Concrete

Due to the very thin walls, 0.25 in to 0.5 in (6.5-13 mm), of the models it is necessary to use a concretious material called micro-concrete. It is not possible to model concrete by merely scaling the individual components, e.g., cement, coarse and fine aggregates, and admixtures according to laws of similitude (19). Limitations on the selection of model concrete, i.e., micro-concrete, are not imposed as long as the overall physical properties of the model material such as the uniaxial stress strain curve and the failure envelope are similar to prototype concrete. Further, it does not matter how these properties are obtained. Designed in a similar manner as concrete in any prototype structure which will display the desired properties at the desired time after casting, the model concrete uses Type I or Type III cement, a water-cement ratio of 0.3-0.6 and a maximum aggregate size determined by similitude and the thickness and reinforcement spacing in the model.

To prevent the necessity of high water/cement ratios to obtain workable mixes the finer particles are limited to less than 10% passing the U.S. No. 100 sieve in model concrete mixes. In addition, an increase in aggregate fineness decreases the strength of model concrete. The constant ratio of paste to aggregate provides inadequate paste to cover the larger surface area caused by the finer aggregates leading to weaker model concrete.

Additional characteristics of micro-concrete and different methods for mix designs are described in References 3, 5, 16, and 19.

Reinforcement

Most deformed bar reinforcement used in prototype structures have a well defined yield point and a relatively long yield plateau. The most commonly used high strength steel, ASTM A432 bars, can be expected to have a nominal

yield strength of 60,000 psi and the sharp yield stress-strain curve. The exceptions are the high strength ASTM A431 bars which have a typically rounded stress-strain curve and a nominal yield strength of 75,000 psi.

Model reinforcement must have the same shape of stress-strain curve as the prototype reinforcement even if non-unity stress and strain are used. The steel must meet the following requirements (5)

1. Stress-strain curve similar to that of prototype, including an appropriate amount of ductility.
2. Desired yield strength
3. Proper bond characteristics.

The reinforcing steel wire to be used here has a diameter of 0.106 in (2.5 mm) and is cold-drawn. It has been annealed to obtained uniaxial stress-strain properties similar to ASTM A432, Grade 60 reinforcing steel. The wire is smooth and no attempt to roughen it is being made as the bond stresses are anticipated to be quite low and rarely predominate in this type of concrete structure.

The method of reinforcing these shell models is by placing the steel wire in a two-way mesh along the ruling line in the center of the shell wall. The steel ratios used vary from 0.3% to 0.9% at the throat which gives a wire spacing for the one-half inch thick shell varying from 5.6 in (142 mm) to 1.9 in (48 mm). The number of wires used in each direction varies from 40 to 120, corresponding to the ratios, respectively in each direction.

A material scale factor of unity between the model and the prototype was used in the designs of the materials used in constructing the shells.

3. Formwork & Construction

The double-walled form for the models is constructed by placing fiber-glass on wires laid out along the shell ruling lines. The 0.08 in (2.0 mm) thick fiberglass material, C-Flex, is a unidirectional fiberglass reinforcement

that is manufactured in long 12 in (0.30 m) wide planks. C-Flex contains rigid rods of pultruded glass reinforced plastic (GRP) on 1/2 in (13 mm) centers which give it a self-supporting nature when spanning an open framework. The rods impact high strength qualities to the structure in the direction which they run due to a very high glass/resin ratio. The spacings between the rigid rods are filled with unsaturated strands of continuous fiberglass coverings, which when saturated become excellent unidirectional reinforcements also. A light fiberglass cloth holds the material and gives C-Flex the ability to bias, which enables it to follow the exact contours of most surfaces and to conform to compound curved shapes.

Sixty wires for each form are supported on a frame shown in Fig. 3. These wires are threaded at each end and connected with hexnuts, so that a tensile force may be applied to the wires.

Two steel rings made of 4 x 3 x 1/4 in. angles for the top ring and 5 x 3 x 1/4 in angles for the bottom ring were used for the wire supports. These are supported on a steel HP 10 x 42 column and the floor. The bottom ring encloses a plywood platform and is about 15 in (0.38 m) above the floor to allow access underneath and easy form removal. See also Fig. 4. Fig. 5 shows in more detail the top and bottom rings with the hole patterns indicated for the form wires. These were located based on the geometry of Fig. 2 and Eq. (12), which gave $\delta=77.898°$. Hole patterns for the shell reinforcing wires, a maximum of 120 wires in each ruling line direction, were found in a similar manner and provided on the rings. The holes are 0.125 in (3.2 mm) diameter to accomodate the No. 12 (0.106 in dia.) wires.

In the construction of the forms the following sequence was followed:

1. Place form wires and tighten as shown in Fig. 6. Due to the ductile nature of the wire, continual monitoring of the wire is necessary to avoid excessive sagging of the fiberglass panels.
2. Precut 54 fiberglass panels for the inner (outer) form to a

length of 60.97 in (61.09 in) for the bottom and middle levels. Twenty additional panels of length 41.62 in (41.70 in) is also required for the top level. Further, an angle of inclination, $\eta = 13.66°$ (13.79°) was cut on each ends of the panel to allow butting of the panels during the construction process. Initially the fiberglass panels GRP ribs were placed in the direction of the form wires and based on the length and angle of inclination calculated, the precut panels discontinued at each lift point. However, due to sagging by selfweight and to provide a stiffer structural network, the panels were later placed in opposition to the form wires at the calculated angle of inclination, $\eta = 13.66°$ (13.70°). This revision and having the precut panels at the desired lengths and angle of inclination expedited further construction of the formwork.

4. Attach the precut panels to the lattice work of form wires by stitching, Fig. 7. It was found from practice that a minimum of five stitches per row was required in securing the panel to avoid a scalloping effect when the panel cured from the application of resin. Further, all seams must be secured.

5. Apply a low-shrink resin to the assembled mold. It is recommended that a low shrinkage polyester (Marble Casting) resin be used for saturating C-Flex planking. As it cures, general purpose laminating resin can shrink considerably and cause distortion if used on the C-Flex layer. The use of marble casting resin eliminates this possibility of distortion. Since most resin are air-inhibited; i.e., the surface of the resin that is in contact with the air will not cure completely and remains tacky, a wax solution was added to the laminating resin during the final coat application to seal the surface of the resin from the air and allow for a com-

plete cure. To provide adequate working time 8 cubic centimeters of catalyst was used per 946.36 cubic centimeters (1 quart) of resin. The use of paint brushes was found best in applying the resin along the curved surface. It is important to note here that once the material is saturated no more resin is required. All the excess will do is add weight, cause the laminate to be brittle, and to shrink excessively. Fig. 8 shows the completed form.

6. After hardening reinforcing ribs of 1/4 in. (6.5 mm) plywood, shown in Fig. 9, are placed along its connecting edges and interior.
7. Label and cut form into prescribed panels, Fig. 10 and 11. A typical panel in detail is shown in Fig. 12.

The sequence for the model construction is the following:

1. Assemble inner form.
2. Assemble reinforcing wires. These include those in a reinforced concrete beam at the top of the shell, Fig. 13. Note that the shell wires are threaded at the top and attached to the top ring with nuts. However, they are simply bent at the bottom ring shown in Fig. 13. Actually they are threaded at the bottom also (despite the Fig.).
3. Assemble first lift of outer form. Spacer pieces made of aluminum tubing 1/2 in (13 mm) long are placed at the four corners to assure proper spacing between forms.
4. Fill lower lift with pumped concrete.
5. Repeat steps 3 and 4 for the other lifts.
6. After curing, remove all forms, and install top plywood cover over the shell.

4. Concrete Pump

Selection of the pump to place the micro-concrete in the forms was based on one which could handle high viscous, high abrasive material without the inducement of air during the pumping action. Further, a minimum pump speed of 5 GPM at a differential pressure of 10 psi was required.

The Moyno Pump selected is a progressing cavity pump. The pumping action is created by the single helical rotor rolling eccentrically in the double threaded helix of the stator. As the rotor turns, the cavities progress from the suction to the discharge. As one cavity diminishes, the opposing cavity increases at exactly the same rate, thus the sum of the two discharges is a constant volume. At a differential pressure of 0 psi the pump speed is rated 6 GPM and 4 GPM at a differential pressure of 80 psi, well within the specification requirements.

A hopper with total capacity of 6 ft^3 (0.17 m^3) was constructed of 0.375 in (9.5 mm) plate metal and placed on the pump. Figure 14 shows the pump and hopper in detail.

5. Loading System

It is intended to test the models under the action of dead and either surface loads or axial compression. Application of multiple point loads is usually done by a level (whiffletree) system which automatically distributes the loads to the various points according to the geometry of the system. The effects of friction must be accounted for.

One of the problems of the rod and lever system is the difficulty of accommodating large changes in geometry without changing the distribution of loads.

The loading arrangement for elastic models of plates and shells are often dead weights hung from strings, in contrast to the hydraulically actuated whiffletree. The load from each string is distributed on the model

surface by a pad or tripod. The weights are easily controlled for the small values of load being applied to these models, with unloading and loading done by raising and lowering a platform which picks up the weights as it is raised.

Uniform loads for shell models are usually applied by an air pressure or vacuum system. Loads are applied normal to the model surface. The vacuum system employed utilizes the platform (Fig. 15) as one surface and the top plate (Fig. 16) comprising the other. The joint between the plate and shell surface is a particular problem, since the plate seal must restrained without at the same time restraining the model edge. To combat this problem a rubber inner tube will be used for the plate seal. The uniform load is applied through suction using a Welch Duo-Seal Vacuum Pump with a flow rate of 5.6 cubic feet per minute and maximum vacuum of 0.8 psi absolute. Four evacuation points are located around the platform.

One advantage of this method is that problems of localized bending associated with concentrated loads are eliminated.

The third loading method already mentioned and commonly used is to apply a pressurized membrane to the shell surface which reacts against the load frame. A disadvantage of this system also is that the loading membrane may stiffen the shell edges.

The support frame will also be designed to accommodate mechanical or hydraulic jacks with fittings at the load end and load cells at the reaction end for models loaded in axial compression.

6. Instrumentation

The response at low loads obtained from strain data will be used to monitor the structure and make comparisons with predicted internal tractions. The location of strain rosettes are shown in Fig. 17. Locations 1,2,15,16 have three element electric-resistance strain rosettes (paper-backed, gage length = 0.32 in) while the other gage locations shown have 2-element

rosettes (paper-backed, gage length = 0.64 in). In addition to these, pairs of gages are spaced around the perimeter of the shell at the throat 90° apart (gages 17-22).

The location of the gages were selected to monitor strain response in a buckled area as buckling commences. It is expected that this method will give a fairly sensitive indication of the buckling load based on previous studies.

Finally, to determine the amount of load taken from the top plate, calculated to be 44%, strain gages (single element) are mounted on the support column.

Dial gages are also employed to monitor lateral shell movement as well as measure initial surface imperfections. These are mounted on a aluminum channel shown in Fig. 17 which can be relocated to different circumferential positions on the shell during the test. The dial gages used all have a least reading of 0.001 in (0.025 mm) and a travel of 1 in or 2 in (2.54 or 50.8 mm).

Probably the most important change in buckling experiments on shells in this decade is the extent of surface imperfections, i.e., thickness variations and deviations from ideal geometry (2,10). To measure the deviations from ideal geometry the dial gages are calibrated and a standard built into the center column as shown in Fig. 17. The bolts shown can be adjusted to correspond to the ideal shell curve. Thickness variations are determined after testing by drilling pilot holes at selected location and thickness measured. The deviations recommended between the theoretical shape of the cooling tower shell and the actual prototype structure should be limited to (23)

$$\Delta r = \frac{\sqrt{rh}}{47.5} \leq 0.10 \text{ m } (3.95 \text{ in}) \tag{37}$$

with r and h being local values of the minimum radius and of the wall thickness of the cooling tower shell. Additionally the error in the slope should be less than 1.5% and has to be corrected gradually in the ensuing construction.

Chapter V

Conclusions

Large natural draft cooling towers are required for dry-type cooling of power plants having high capacity. For these structures reinforced concrete is still the ideal material if important aspects of the shape and construction of the hyperbolic veil are considered.

Design and construction of support facilities for micro-concrete model shells, hyperboloids of revolution are presented. Motivation for the study was based on

1. Better understanding of buckling behavior and the primary factors affecting it.
2. To obtain better inputs for computations.
3. To obtain correlation factors between analysis and test and for the material effects.

The shell model was proportioned such that failure would be initiated by buckling. Further considerations were that the wall thickness must be 0.25 (6.5 mm) to 0.5 in (13 mm) so as not to preclude steel placement with sufficient cover and adequate steel ratio and the remaining dimensions should give proportions based on previous studies as given in Table 1. The final dimensions selected were an overall shell height, H=12 ft (3.65 m); shell throat radius, a=3 ft (0.91 m); shell thickness, h=0.25 to 0.5 in (6.5-13 mm); and shell geometry parameter, b = 7.55 ft (2.30 m).

The use of the most striking property of the hyperboloid of one sheet, i.e., ruling lines, to aid in the construction of the formwork and placement of steel reinforcement has proven to be a very novel and convenient scheme.

A fairly simple system for mointoring surface displacements under the action of dead and either surface loads or axial compression and for measuring initial surface imperfections is described.

It is intended that a total of eight models with varying support conditions, thickness, loading conditions and reinforcement configurations be constructed and tested in the future. With the support facilities and text described herein as a foundation, it is hoped that future details on various aspects of materials and results will be forthcoming in order to gain a clearer perception of the buckling behavior of shells.

Appendix I: Tables

Table 1. Proportions of Buckled Shells

Reference	$\frac{H}{a}$	$\frac{a}{h}$	$\frac{a}{b}$
6	4.54	198	----
7,8	3.9	202	0.401
15	3.9	175	0.436
22	4.14	121 to 177	0.283 to 0.447
21	4.5	204	0.333
23	4.19	123 to 269	0.517
11	3.9	91 to 615	0.400
17	6	100 to 182	0.373

H = overall shell height, a = shell throat radius,

h = shell thickness, b = shell geometry paramters.

Table 2. Computed Shell Buckling Loads

h, in (mm)	z, in (cm)		q_{cr}, psi (kPa)
0.5 (13)	0 (0)	Throat	20.2 (139)
	36 (91)		18.5 (127)
	108 (274)	Base	12.4 (85)
0.375 (10)	0 (0)	Throat	11.1 (76)
	36 (91)		10.2 (70)
	108 (274)	Base	6.8 (47)
0.25 (6)	0 (0)	Throat	4.6 (32)
	36 (91)		4.2 (29)
	108 (274)	Base	2.8 (19)

Note: f'_c = 4000 psi (27.6 MPa); ε_o = 0.002 in/in (m/m)

Table 3. Shell Membrane Stresses

		h = 0.5in (13mm) g = 0.0434 psi q = 18.5 psi (127 kPa)		h = 0.375in (10mm) g = .03255 psi q = 10.2 psi (70 kPa)		h = 0.25in (6mm) g = 0.0217 psi q = 4.2 psi (29 kPa)	
		σ_ϕ, psi (kPa)	σ_θ, psi (kPa)	σ_ϕ, psi (kPa)	σ_θ, psi (kPa)	σ_ϕ, psi (kPa)	σ_θ, psi (kPa)
z = 0 Throat	g[a]	-3 (-21)	-0.5 (-3)	-3 (-21)	-0.5 (-3)	-3 (-21)	-0.5 (-3)
	q[b]	105 (723)	-1317 (-9074)	77 (532)	-967 (-6663)	48 (331)	-602 (-4148)
	P	-429 (-2956)	-68 (-469)	-315 (-2170)	-50 (-344)	-196 (-1350)	-31 (-214)
	Total	-327 (-2253)	-1385 (-9543)	-241 (-1660)	-1017 (-7007)	-151 (-1040)	-633 (-4361)
z = 108 in (274 cm) Base	g[a]	-10 (-69)	-2 (-14)	-10 (-69)	-2 (-14)	-10 (-69)	-2 (-14)
	q[b]	-565 (-3893)	-2202 (-15172)	-415 (-2859)	-1616 (-11134)	-258 (-1778)	-1007 (-6938)
	P	-288 (-1984)	-17 (-117)	-212 (-1461)	-13 (-90)	-132 (-909)	-8 (-55)
	Total	-863 (-5946)	-2221 (-15303)	-636 (-4382)	-1631 (-11238)	-400 (-2756)	-1016 (-7000)

a. Dead load g based on assumed unit weight of microconcrete of 150 lb/ft^3 (23.8 kN/m^3)

b. Buckling load q based on assumption of critical location at 36 in (91 cm) below throat.

Appendix II: Figures

THIS BOOK CONTAINS NUMEROUS PAGES WITH DIAGRAMS THAT ARE CROOKED COMPARED TO THE REST OF THE INFORMATION ON THE PAGE.

THIS IS AS RECEIVED FROM CUSTOMER.

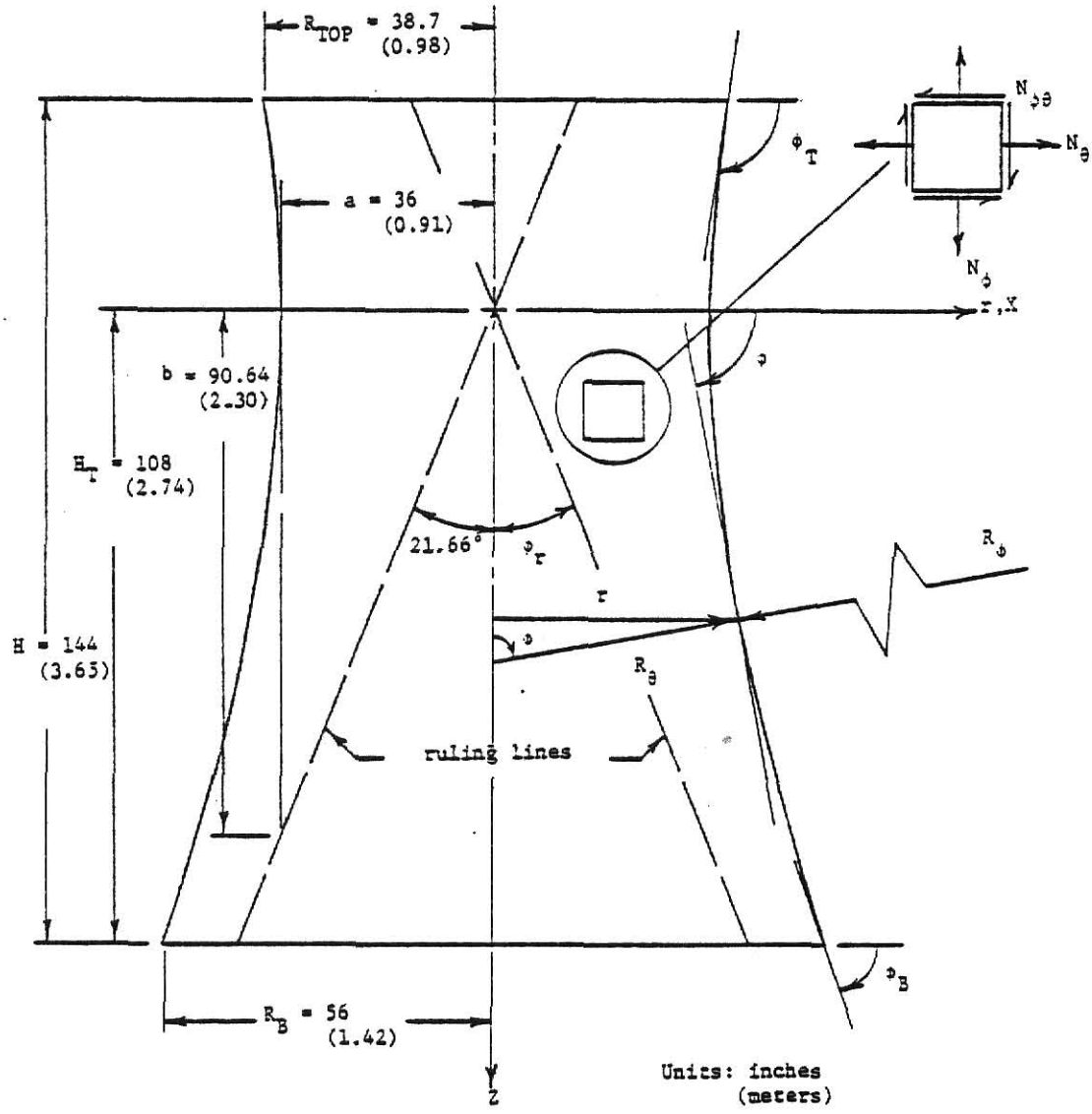

Fig. 1. Shell Geometry

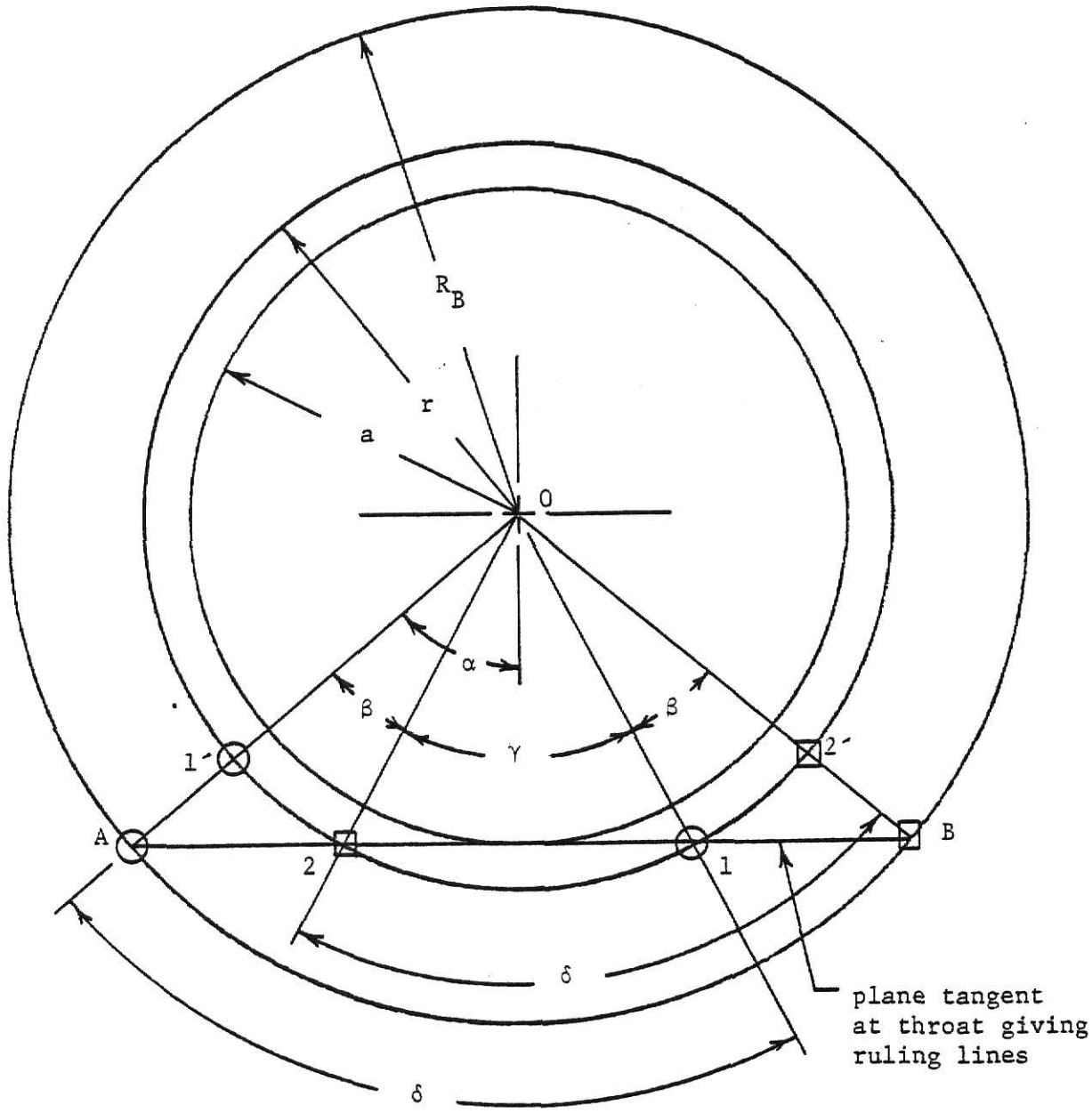

Fig. 2. Hole Geometry For Locating Ruling Lines

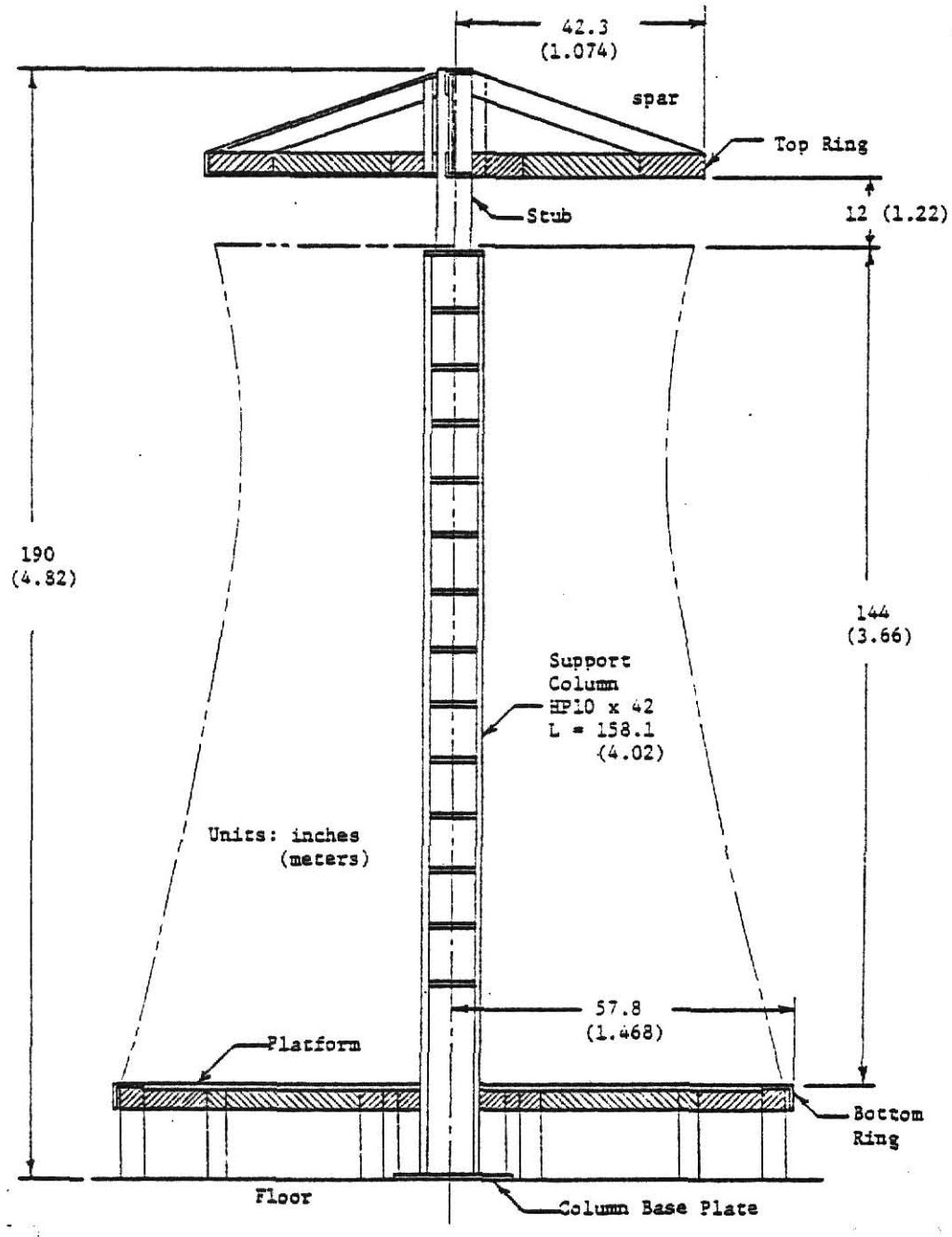

Fig. 3. Support Frame

THIS BOOK CONTAINS SEVERAL DOCUMENTS THAT ARE OF POOR QUALITY DUE TO BEING A PHOTOCOPY OF A PHOTO.

THIS IS AS RECEIVED FROM CUSTOMER.

THIS BOOK CONTAINS NUMEROUS PICTURES THAT ARE ATTACHED TO DOCUMENTS CROOKED.

THIS IS AS RECEIVED FROM CUSTOMER.

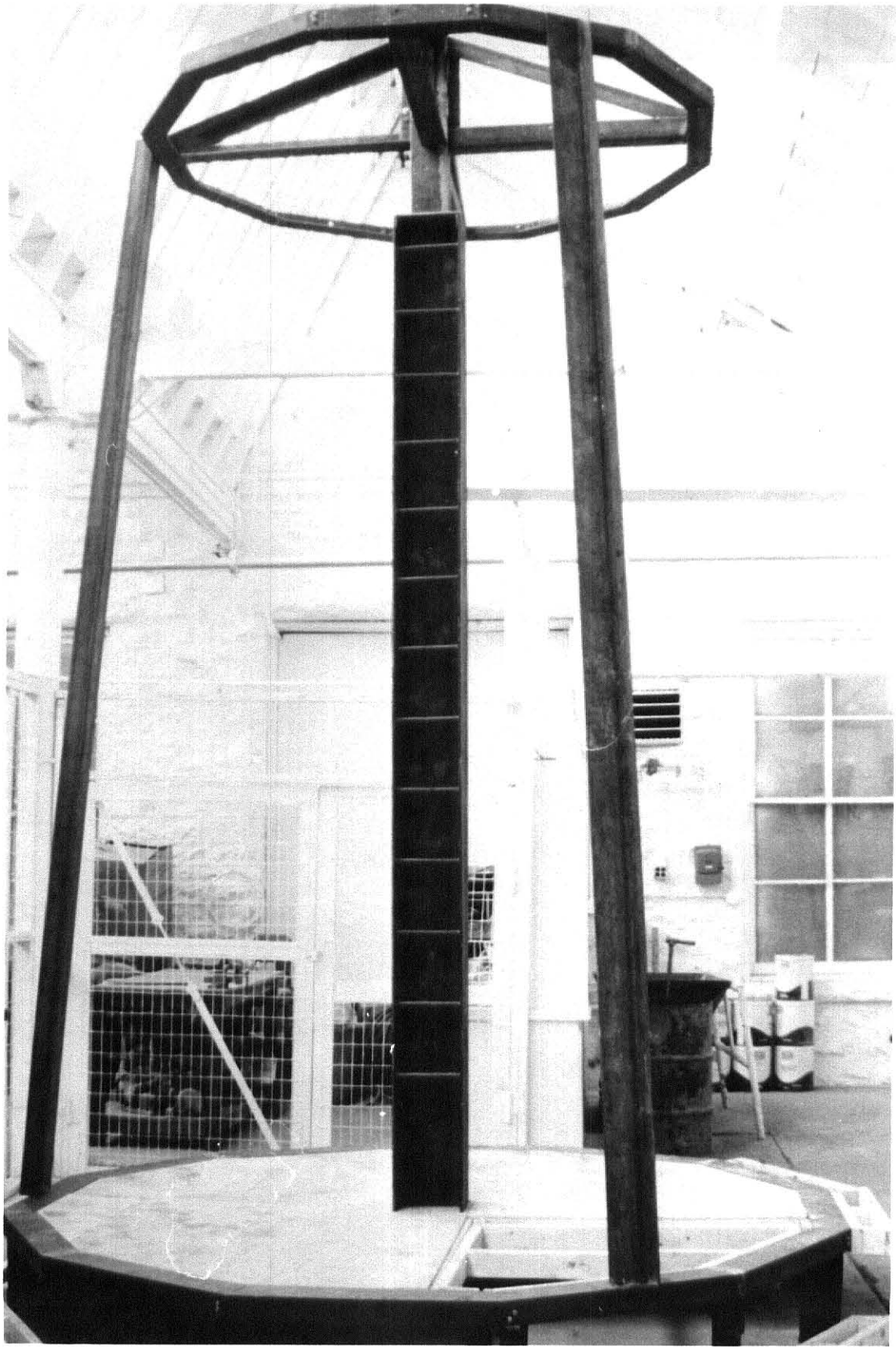

Fig. 4 Support Frame and Platform

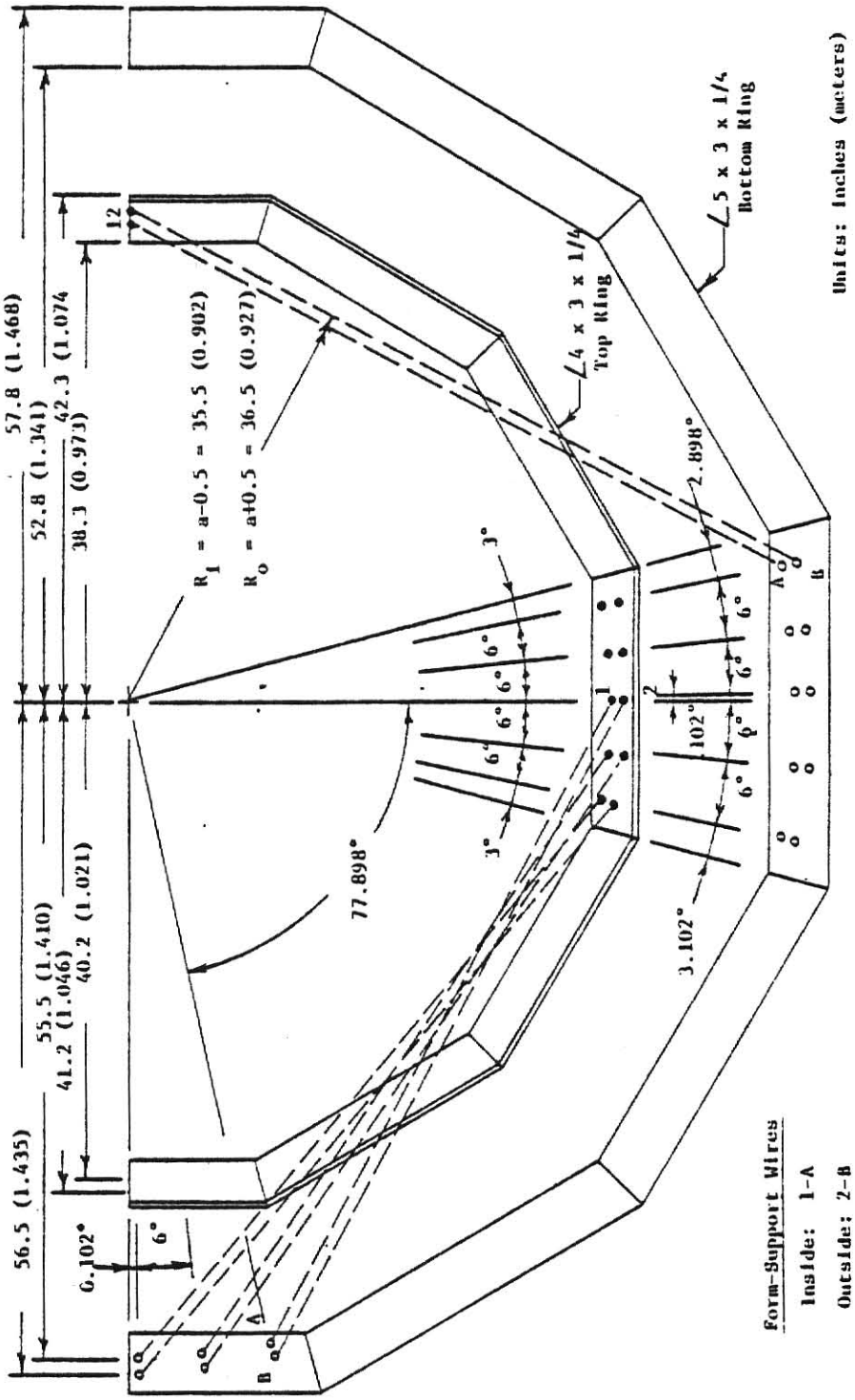

Fig. 5. Support Rings With Hole Patterns for Form-Support Wires

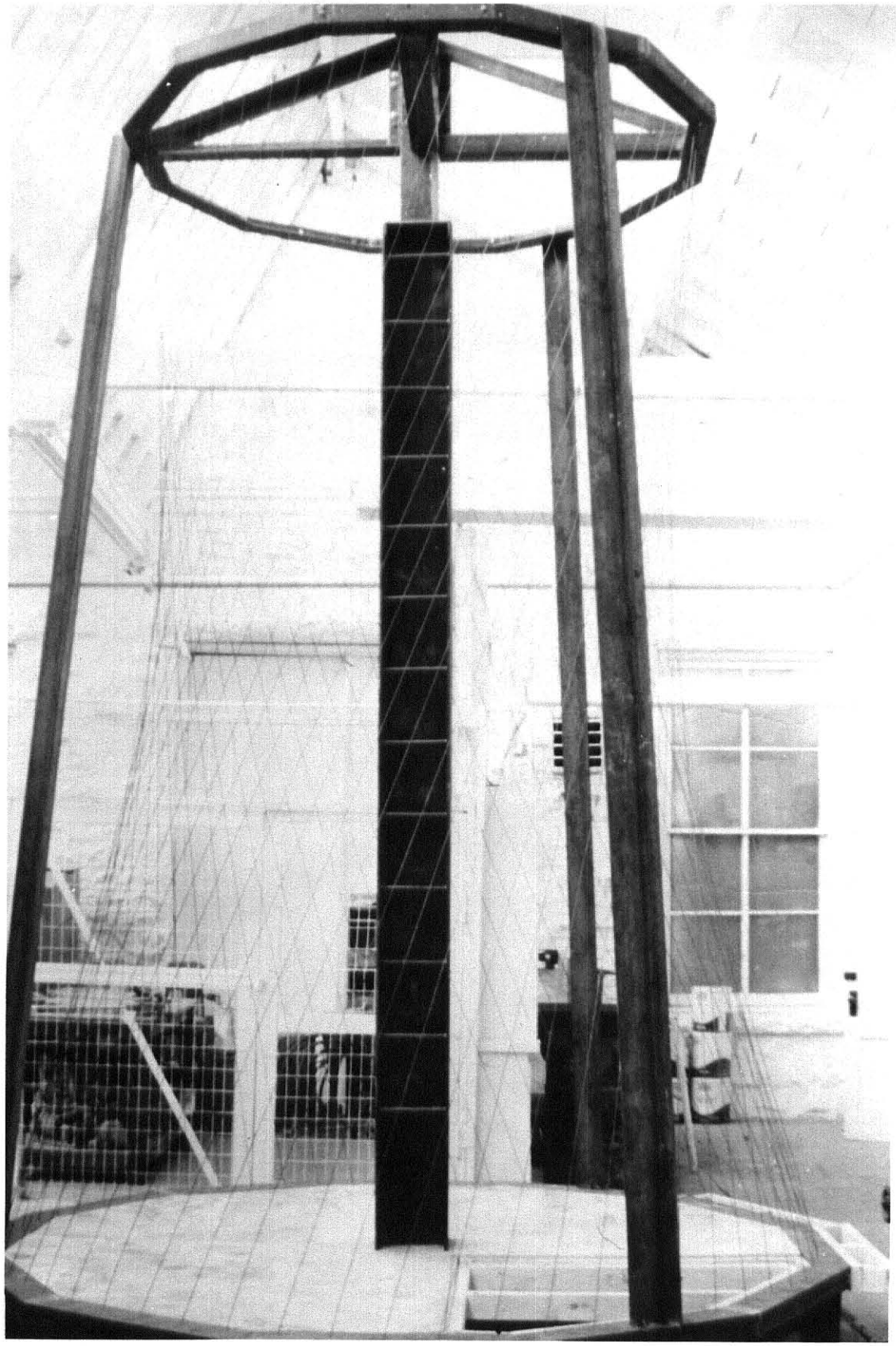

Fig. 6 Form Wires in Place

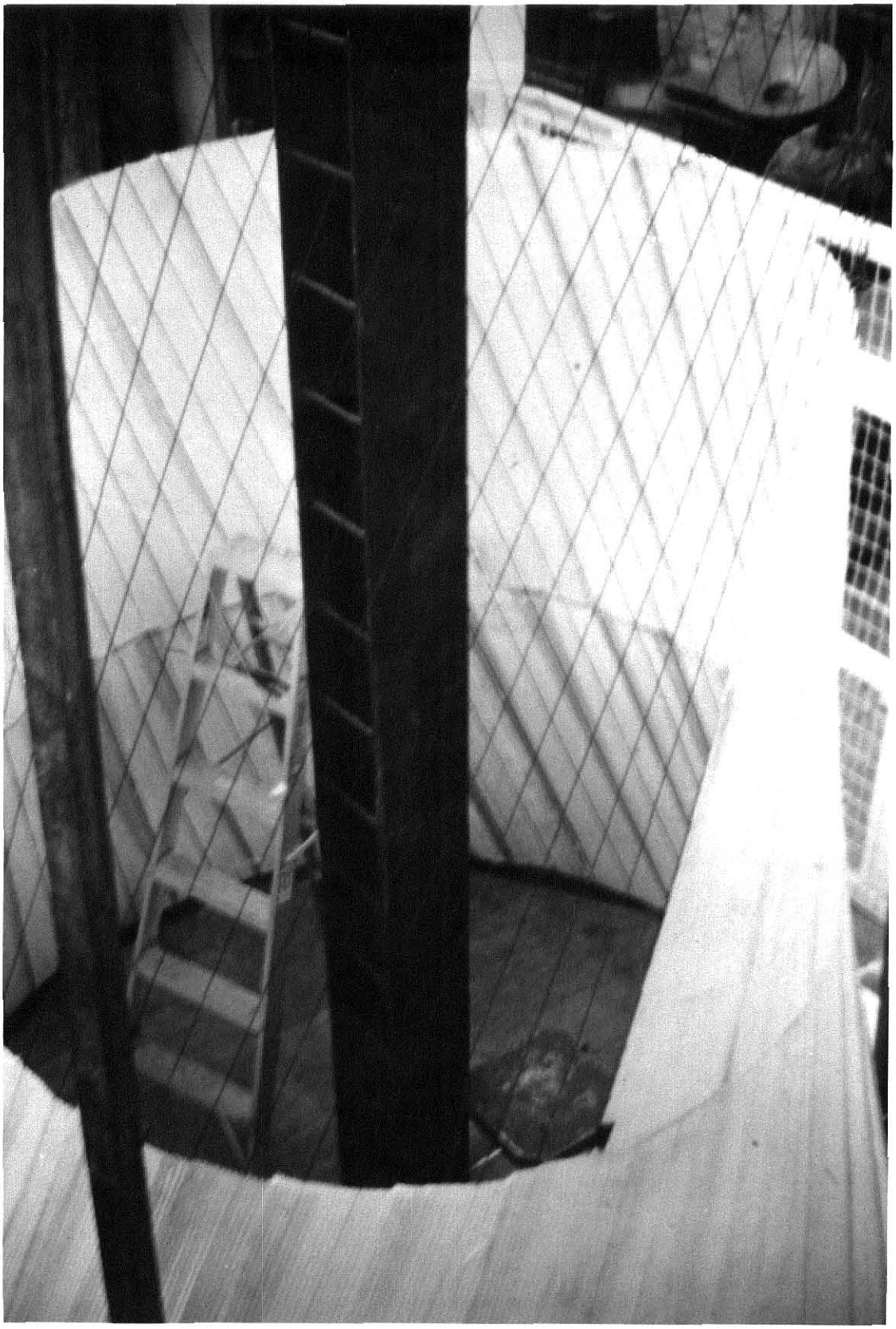

Fig. 7 Panels on Wires

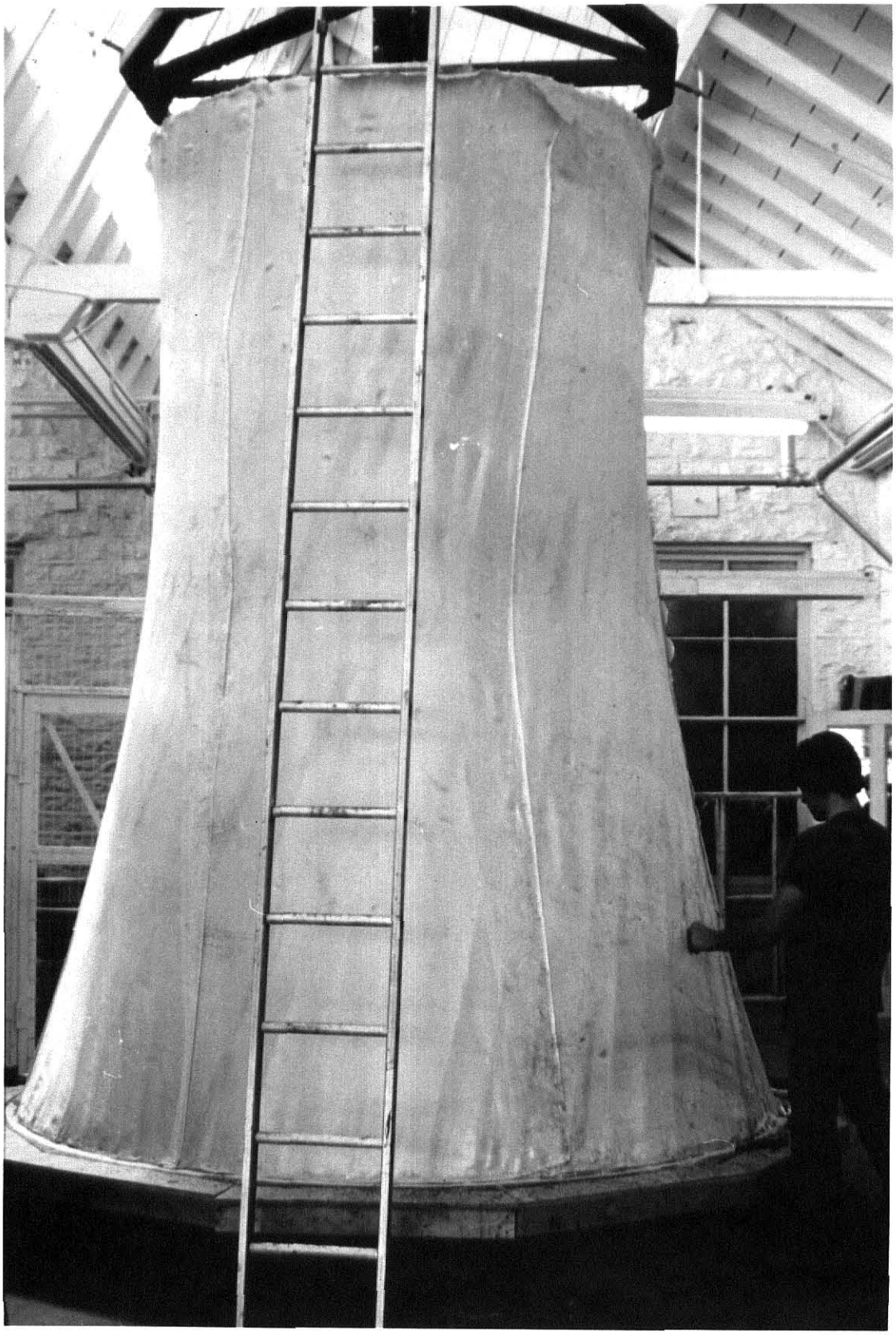

Fig. 8 Completed Form

Fig. 9 Stiffening Ribs In Place

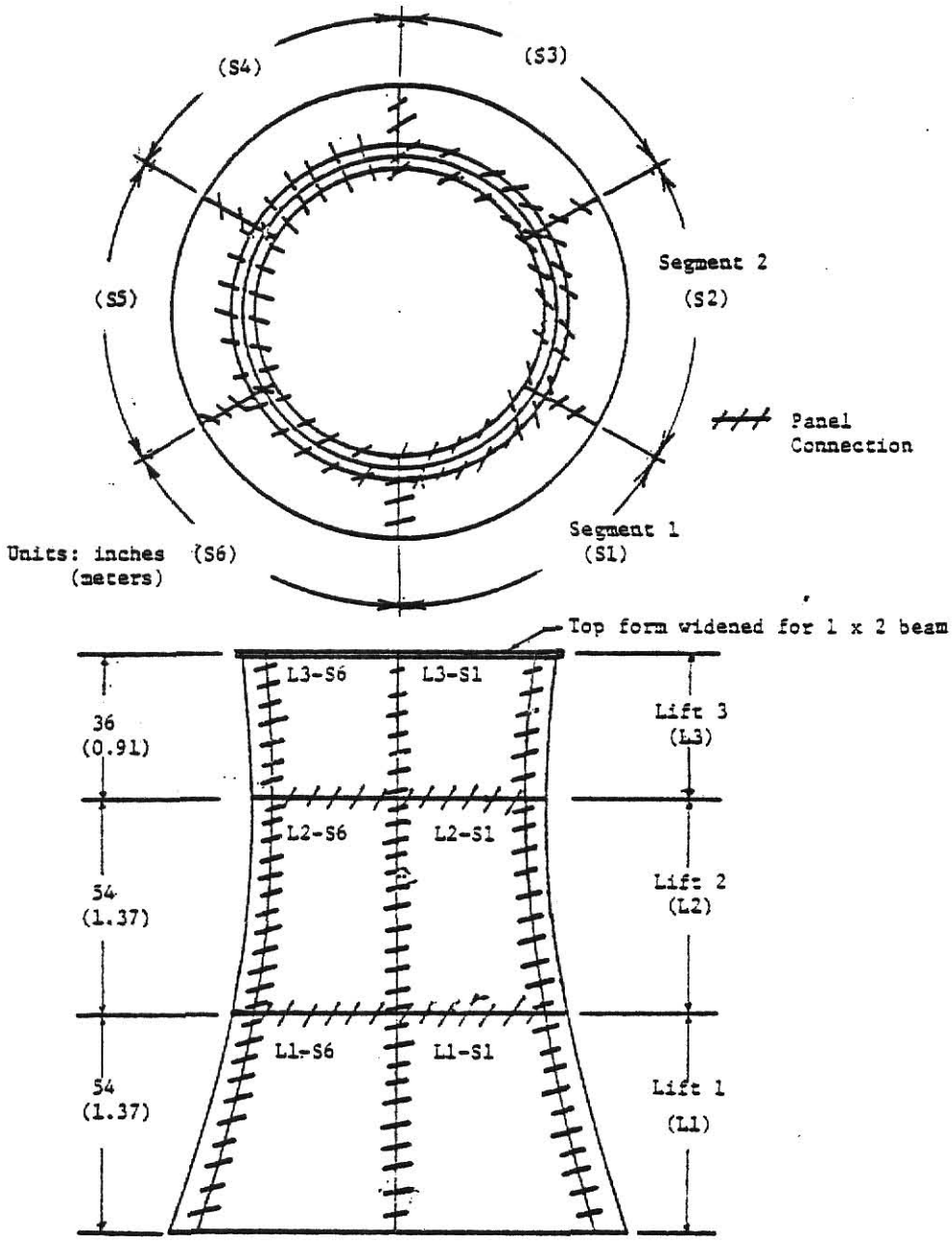

Fig. 10. Formwork Panel Layout

Fig. 11 Cut Out Section

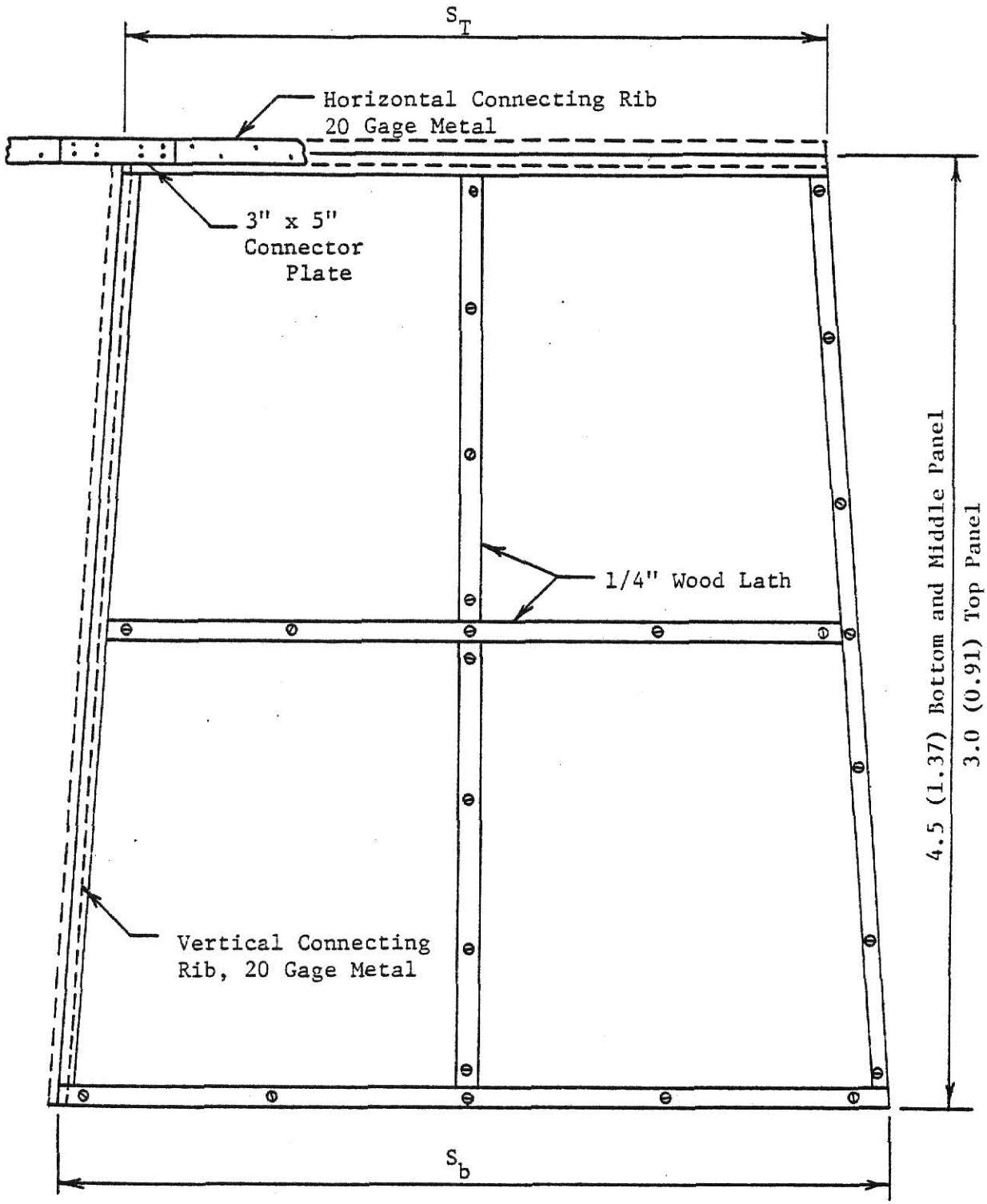

S_T and S_b vary per level of interest.

Units: feet
(meters)

Fig. 12. Typical Panel

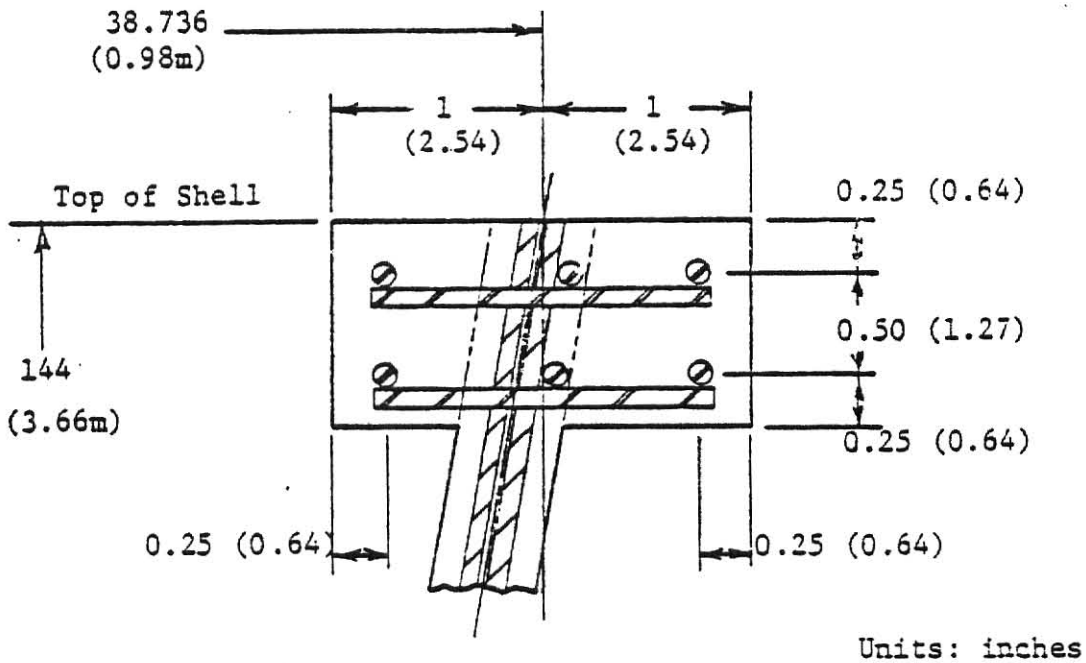

a. Upper Edge Stiffening Beam

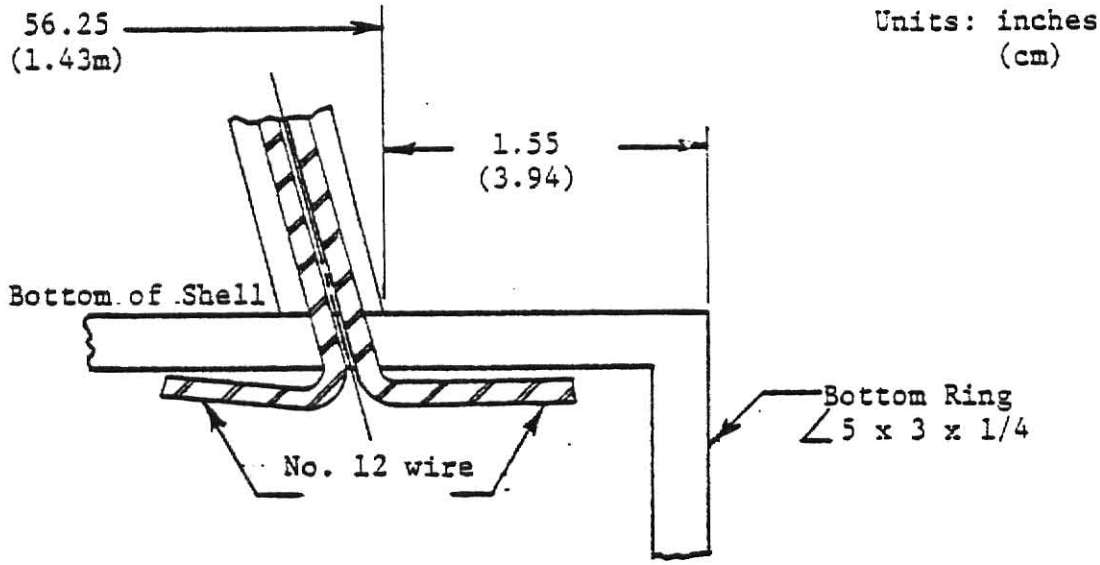

b. Lower Edge Reinforcing Wire Connection

Fig. 13. Boundary Details

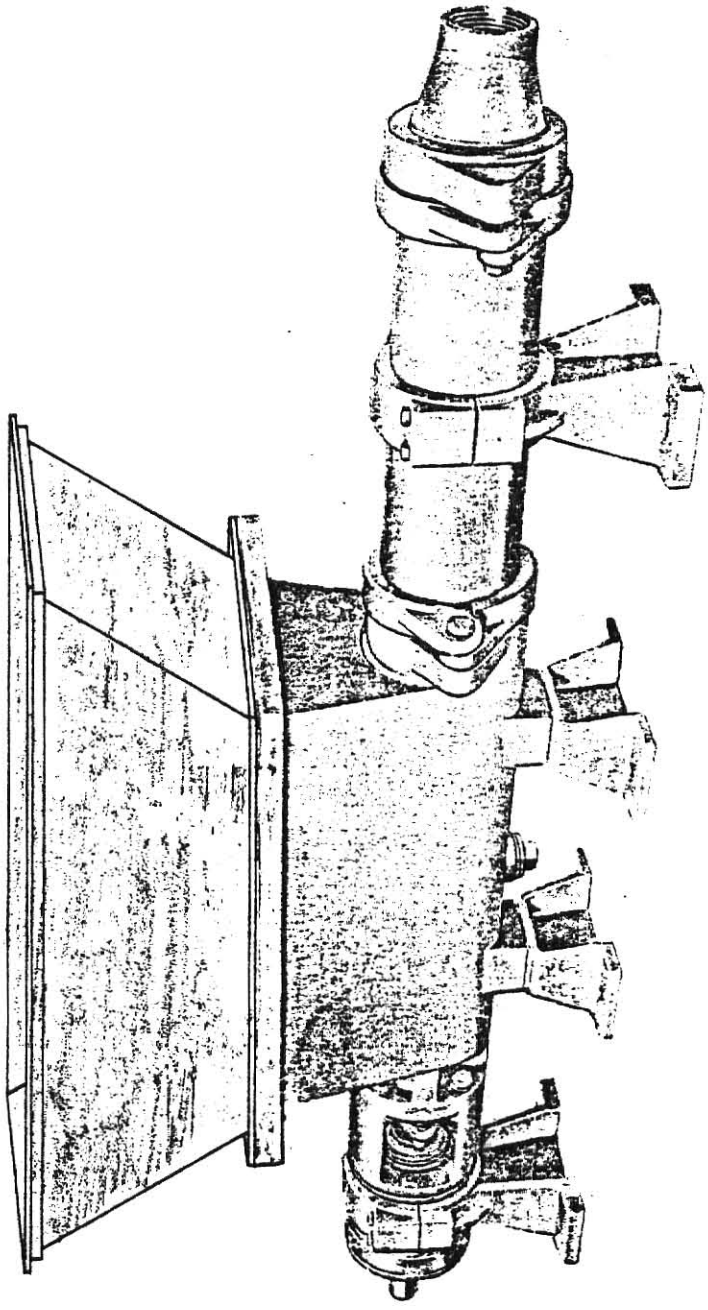

Fig. 14. Moyno Pump and Hopper

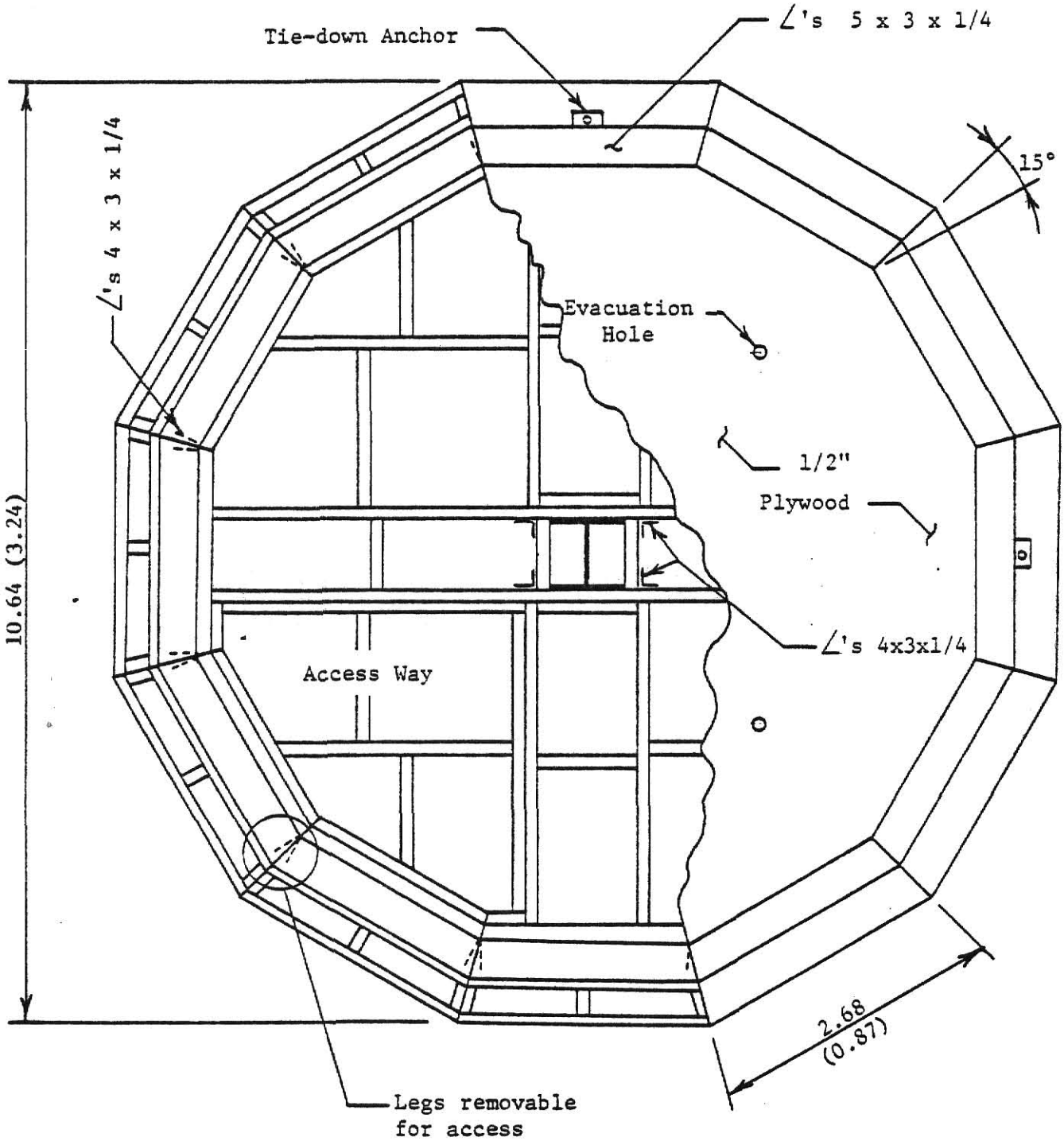

Units: feet
(meter)

Fig. 15 Platform Detail

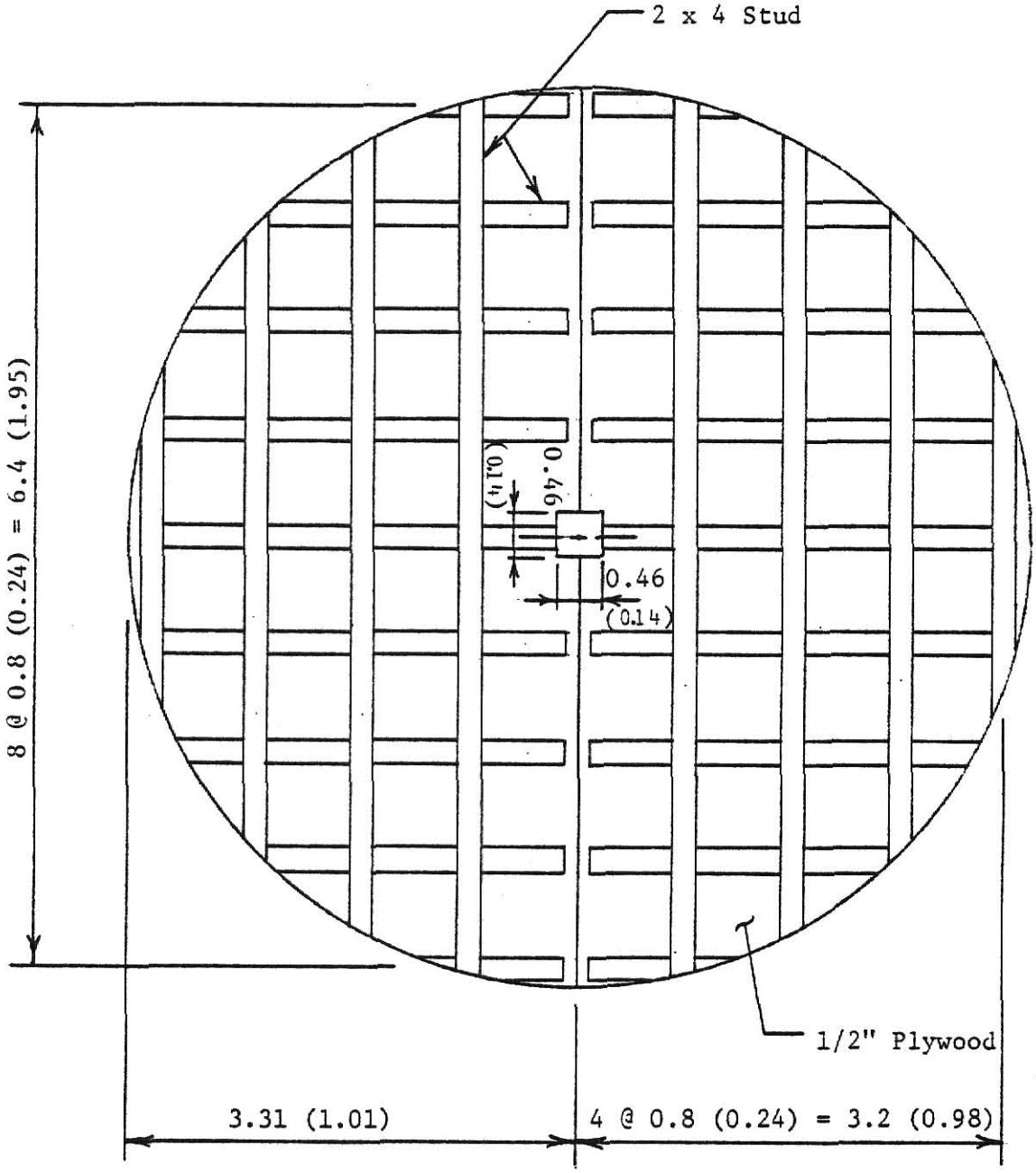

Fig. 16. Top Plate

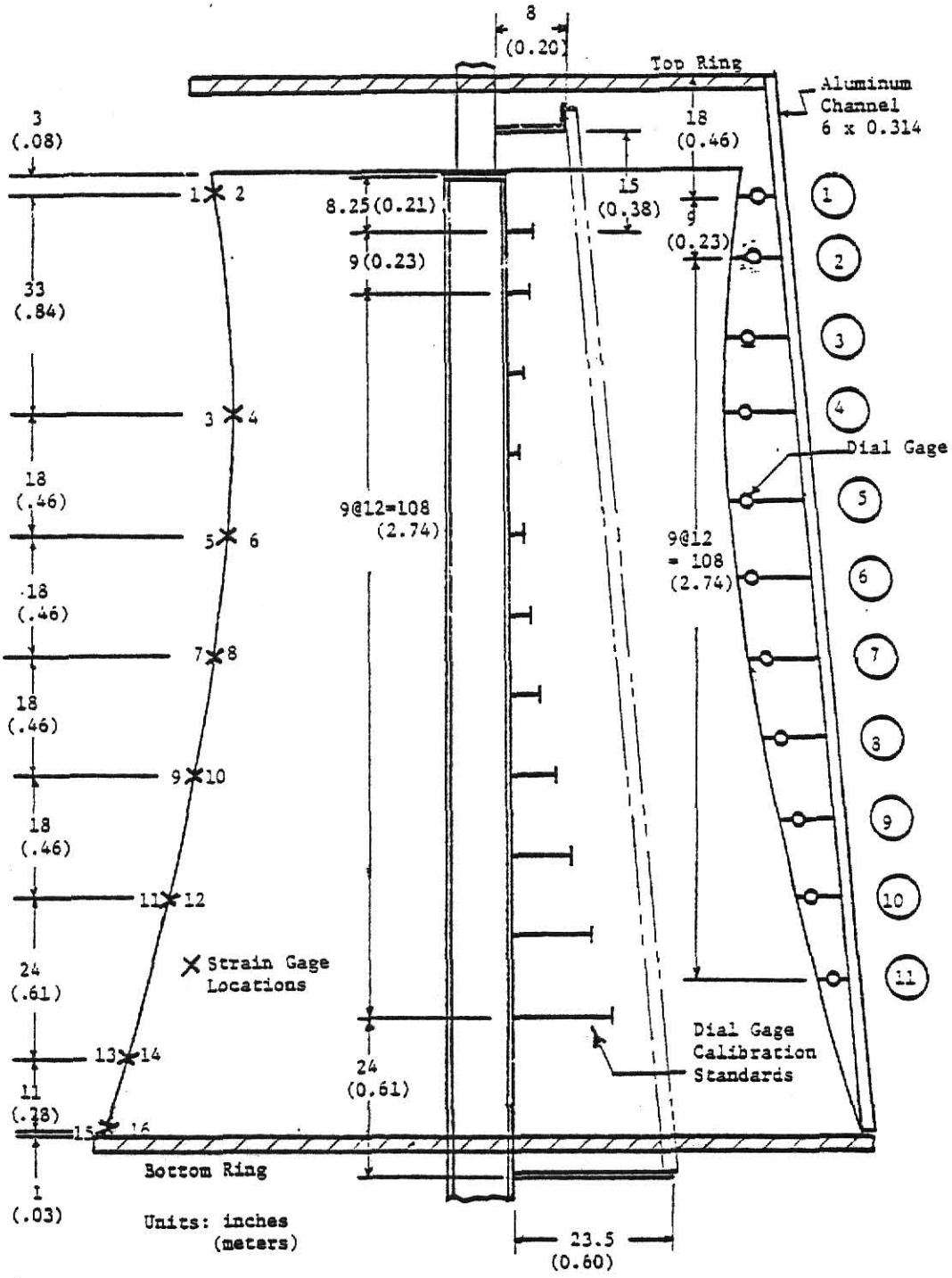

Fig. 17. Strain Gage and Displacement Gage Locations

Appendix III: Notations

Notations

a - throat radius

b - shell geometry parameter

E - Young's Modulus

E_T - Tangent Modules

F_θ, F_ϕ - experimental correction factors depending on the shape of the cooling tower shell

f'_c - concrete uniaxial compressive strength

g - dead weight per unit area of surface

h - shell thickness

H - shell height

H_T - vertical distance from the throat to the base

$K_{G\theta}, K_{G\phi}$ - factors depending on shape and boundary conditions of the cooling tower shell

L - length of ruling line

P - applied axial load

P_θ, P_ϕ, P_n - load components per unit area of middle surface

q - uniform external pressure

q_{cr} - pressure at which buckling commences

Q_θ, Q_ϕ - geometry buckling parameters

r - horizontal radius

R_B - base radius

R_T - top radius

Δr - deviation recommended between theoretical shape and actual prototype structure.

Z - vertical coordinate

ε_o - associated strain for concrete

ν - Poission's Ratio

Acknowledgements

The writer would like to acknowledge the assistance rendered by Dr. Stuart E. Swartz, Professor of Civil Engineering, during the course of the project and preparation of this thesis.

Sincere thanks are also extended to Professor K. K. Hu for his valuable advice and to Dr. Robert Snell, Head, Department of Civil Engineering, for his continual support.

Appreciation is also due to Mr. Russell L. Gillespie for his help while working in the Civil Engineering Design Shops and to the Department of Civil Engineering for providing the facilities.

Thanks also to Arthur C. Munoz and LeAnn F. Runyan for their assistance and encouragement in the construction of the support facilities.

The research reported herein was supported in part by the National Science Foundation, Grant ENG-7818415. This support is gratefully acknowledged.

Bibliography

1. ACI-ASCE Committee 334, "Reinforced Concrete Cooling Tower Shells-Practice and Commentary," ACI Journal, Vol. 74, No.1, Jan. 1977.

2. Al-Dabbagh, Adam and Gupta, Ajaya K., "Meridional Imperfection in Cooling Tower Design," Journal of the Structural Division, ASCE, Vol. 105, No. ST6, June 1979.

3. Aldridge, Weldon W. and Breen, John F., "Useful Techniques in Direct Modelling of Reinforced Concrete Structures," Models for Concrete Structures, Publication SP-24, American Concrete Institute, Detroit, Mich., 1970.

4. Almannai, A., Basar, Y. and Mungan, I., "Beuluntersuchungen an Rotationsschalen-Theorie und Versuch," Bauingenieur, Vol. 54, pp. 205-211, 1979.

5. Carpenter, James E., Roll, Frederic, and Zelman, Maier I., "Techniques and Materials for Structural Models," Models for Concrete Structures, Publication SP-24, American Concrete Institute, Detroit, Mich., 1970.

6. Central Electricity Generating Board, "Report of the Committee of Inquiry into Collapse of Cooling Towers at Ferrybridge," London England, Nov., 1965.

7. Chan, A.S.L. and Firmin, A., "The Analysis of Cooling Towers by the Matrix Finite Element Method. Part I: Small Displacement," The Aeronautical Journal of the Royal Aeronautical Society, Vol. 74, No. 10, Oct., 1970.

8. Chan, A.S.L. and Firmin, A., "The Analysis of Cooling Towers by the Matrix Finite Element Method. Part II: Large Displacements," The Aeronautical Journal of the Royal Aeronautical Society, Vol. 74, No. 12, Dec. 1970.

9. Cole, Peter P., Abel, John E., and Billington, David P., "Buckling of Cooling-Tower Shells: State-of-the-Art," Journal of the Structural Division, ASCE, Vol. 101, No. ST6, June 1975.

10. Croll, J.G.A. and Kemp, K. O., "Specifying Tolerance Limits for Meridional Imperfections in Cooling Towers," ACI Journal, Vol. 76, No. 1, Jan. 1979.

11. Der, T.J. and Fidler, R., "A Model Study of the Buckling Behavior of Hyperbolic Shells," Proceedings, Institution of Civil Engineers, Vol. 41, Sept., 1968.

12. Gates, T. E., Hu, K. K., McDonald, C. R., and Swartz, S. E., "Construction and Testing of Micro-Concrete Models of Cooling-Tower Shells," Society For Experimental Stress Analysis, Paper No. A80-4 May, 1980.

13. I.A.S.S. Working Group Number 3, "Recommendations for the Design of Hyperbolic or Other Similarly Shaped Cooling Towers," International Association for Shell and Spatial Structures, Brussels, 1977.

14. Kennedy, Berry, "Construction Manual For Custom GRP Fabrication With C-Flex Fiberglass Planking," C/Flex, Seeman Plastic, Inc., 1977.

15. Langhaar, Henry L., Boresi, Arthur P., and Miller, Robert E., "Stability of Hyperboloidal Cooling Towers," Journal of the Engineering Mechanics Division, ASCE, Vol. 96, No. EMS, Oct., 1970.

16. McDonald, C. R. and Swartz, S. E., "Use of Strain Gages On Miniature Concrete Cylinders," Presented at the 1980 SESA Fall Meeting, Ft. Lauderdale, FL., Oct. 12-15, 1980.

17. Mungan, Ihsan, "Buckling Stress States of Hyberboloidal Shells," Journal of the Structural Division, ASCE, Vol. 102, No. ST10, Oct. 1976.

18. Ramaswany, G. S., Design and Construction of Concrete Shell Roofs, McGraw-Hill Book Co., New York, 1968.

19. Sabnis, Gajanan M. and Mirza, Saeed M., "Size Effects in Model Concretes," Journal of the Structural Division, ASCE, Vol. 105, No. ST6, June, 1979.

20. Timoshenko, S. and Woinowsky-Krieger, S., Theory of Plates and Shells, McGraw-Hill Book Co., New York, 2nd Ed., 1959.

21. Veronda, Daniel R. and Weingarten, Victor I., "Stability of Hyperboloidal Shells," Journal of the Structural Division, ASCE, Vol. 101, No. ST7, July, 1975.

22. Yeh, C.H. and Shieh, W.Y.J., "Stability and Dynamic Analysis of a Cooling Tower," Journal of the Power Division, ASCE, Vol. 99, No. PO2, Nov., 1973.

23. Zerna, Wolfgang and Mungan, Ihsan, "Construction and Design of Large Cooling Towers," Journal of the Structural Division, ASCE, Vol. 106, No. ST2, Feb., 1980.

DESIGN AND CONSTRUCTION OF SUPPORT FACILITIES FOR MICRO-CONCRETE MODEL SHELLS, HYPERBOLOIDS OF REVOLUTION

by

Thomas Edward Gates
B.S. Kansas State University, 1979

An Abstract of a Master's Thesis

submitted in partial fulfillment of the

requirements for the degree

MASTER OF SCIENCE

Department of Civil Engineering

Kansas State University
Manhattan, Kansas

1981

Abstract

Design and construction of the support facilities required for the casting and testing of reinforced micro-concrete models of hyperboloids of revolution are discussed. Proportioned such that buckling will occur prior to general collapse, the models are 12 ft. (3.65 m) high, 9.33 ft. (2.84 m) in diameter at the base, and 0.5 in (13 mm) thick.

The eight shell models to be constructed and tested, using the support facilities, will have varying support conditions, loading conditions, and reinforcement configurations.